RESEARCH ARTICLE

CTR-FAPI PET Enables Precision Management of Medullary Thyroid Carcinoma

Ziren Kong[1], Zhu Li[2], Xi-Yang Cui[3], Jian Wang[1], Mengxin Xu[3], Yang Liu[1], Junyi Chen[4], Song Ni[1], Zongmin Zhang[1], Xiaowei Fan[3], Jiazhao Huang[3], Yansong Lin[5], Yuning Sun[1], Yuqin He[1], Xinfeng Lin[2], Tianyu Meng[2], Han Li[1], Yixuan Song[1], Boshizhang Peng[1], Changming An[1], Chenyan Gao[3], Nan Li[2], Chen Liu[2], Yiming Zhu[1], Zhi Yang[2], Zhibo Liu[2,3,4,6], and Shaoyan Liu[1]

ABSTRACT Medullary thyroid carcinoma (MTC) can only be cured through the excision of all metastatic lesions, but current clinical practice fails to localize the disease in 29% to 60% of patients. Previously, we developed a fibroblast activation protein inhibitor (FAPI)-based covalent targeted radioligand (CTR) for improved detection sensitivity and accuracy. In this first-in-class clinical trial, we head-to-head compared [^{68}Ga]Ga-CTR-FAPI PET-CT and [^{18}F]fluorodeoxyglucose ([^{18}F]FDG) PET-CT in 50 patients with MTC. The primary endpoint was the patient-based detection rate, with [^{68}Ga]Ga-CTR-FAPI exhibiting higher detection than [^{18}F]FDG (98% vs. 66%, $P = 0.0002$). This improved detection was attributed to increased tumor uptake (maximum standardized uptake value = 11.71 ± 9.16 vs. 2.55 ± 1.73, $P < 0.0001$). Diagnostic accuracy, validated on lesions with gold-standard pathology, was greater for [^{68}Ga]Ga-CTR-FAPI compared with [^{18}F]FDG (96.7% vs. 43.3%, $P < 0.0001$). Notably, the management of 32% of patients was altered following [^{68}Ga]Ga-CTR-FAPI PET-CT, and the surgical plan was changed for 66.7% of patients. Overall, [^{68}Ga]Ga-CTR-FAPI PET-CT provided superior detection and diagnostic accuracy compared with [^{18}F]FDG PET-CT, enabling precision management of patients with MTC.

SIGNIFICANCE: In this first-in-class clinical trial of CTR, [^{68}Ga]Ga-CTR-FAPI demonstrated an improved patient-based detection rate (98%), tumor uptake (maximum standardized uptake value = 11.71 ± 9.16), and pathology-validated diagnostic accuracy (96.7%) compared with the currently approved method in MTC treatment. It directly altered management in 32% of patients, enabling precision diagnosis and management of MTC.

See related commentary by Witney, p. 264

INTRODUCTION

Medullary thyroid carcinoma (MTC) is a neuroendocrine tumor arising from the parafollicular neuroendocrine cells (C cells) of the thyroid gland (1–3). Although MTC accounts for only 1% to 4% of primary thyroid neoplasms, it contributes to 13% to 15% thyroid cancer–related death (4, 5). Calcitonin, a polypeptide produced by C cells, exhibits excellent sensitivity and specificity for MTC and serves as the most important biomarker for evaluating disease burden and therapeutic efficacy (6, 7). A biochemical cure, defined as a return to normal serum calcitonin levels, is regarded as the strictest curative level for MTC (7, 8). Surgery remains the only curative option for MTC (7); however, 25% to 62% of patients continue to exhibit biochemical persistent disease (in which serum calcitonin does not return to normal) despite undergoing thyroidectomy and aggressive neck dissection (6, 9, 10).

The clinical management of MTC encounters multiple challenges: (i) MTC may present regional or distant metastases at any stage, yet current imaging modalities cannot fully map the extent of disease. Although ultrasound, CT, MRI, and PET-CT with various tracers have been proposed, single-image modality fails to localize disease in 29% to 60% of patients with persistent disease. (11–15), and 16% to 28% of patients remain undetectable by the combination of multiple imaging methods (16–19). (ii) There is no consensus regarding the appropriate surgical extent for MTC. Latent lymph node metastasis may exist in the ipsilateral neck, contralateral neck, and upper mediastinum when serum calcitonin exceeds 20, 200, and 500 pg/mL, respectively (6), which establishes a theoretical foundation for performing prophylactic lymph node dissection based on serum calcitonin levels. However, recent studies suggest that prophylactic lateral neck dissection

[1]Department of Head and Neck Surgery, National Cancer Center/National Clinical Research Center for Cancer/Cancer Hospital, Chinese Academy of Medical Sciences and Peking Union Medical College, Beijing, China. [2]Key Laboratory of Carcinogenesis and Translational Research, Department of Nuclear Medicine, Peking University Cancer Hospital and Institute, Beijing, China. [3]Changping Laboratory, Beijing, China. [4]Beijing National Laboratory for Molecular Sciences, Radiochemistry and Radiation Chemistry Key Laboratory of Fundamental Science, NMPA Key Laboratory for Research and Evaluation of Radiopharmaceuticals, Key Laboratory of Bioorganic Chemistry and Molecular Engineering of Ministry of Education, College of Chemistry and Molecular Engineering, Peking University, Beijing, China. [5]Department of Nuclear Medicine, Peking Union Medical College Hospital, Chinese Academy of Medical Sciences and Peking Union Medical College, Beijing, China. [6]Peking University-Tsinghua University Center for Life Sciences, Beijing, China.

Z. Kong, Z. Li, and X.-Y. Cui contributed equally to this article.

Corresponding Authors: Zhi Yang, Key Laboratory of Carcinogenesis and Translational Research, Department of Nuclear Medicine, Peking University Cancer Hospital and Institute, No. 52 Fucheng Road, Haidian District, Beijing 100142, China. E-mail: pekyz@163.com; Zhibo Liu, Beijing National Laboratory for Molecular Sciences, Zhongguancun North 2nd Street, Haidian District, Beijing 100084, China. E-mail: zbliu@pku.edu.cn; and Shaoyan Liu, Department of Head and Neck Surgery, National Cancer Center/National Clinical Research Center for Cancer/Cancer Hospital, Chinese Academy of Medical Sciences and Peking Union Medical College, No. 17, Panjiayuannanli, Chaoyang District, Beijing 100021, China. E-mail: shaoyanliu.bj@263.net

Cancer Discov 2025;15:316–28

doi: 10.1158/2159-8290.CD-24-0897

in patients without clinically apparent lateral neck disease does not improve biochemical cure rate or patient survival (9, 10). As a result, the debate continues regarding whether MTC surgery should be performed solely based on preoperative imaging or whether prophylactic lymph node dissection is warranted (7). (iii) Patients with unresectable disease lack an efficient treatment strategy. Although targeted therapies, including multitarget tyrosine kinase inhibitors (e.g., cabozantinib and vandetanib) and selective RET proto-oncogene (RET) inhibitors (e.g., selpercatinib and pralsetinib), are recommended for progressive unresectable disease (20–24), available studies with long-term follow-up have not demonstrated improved overall survival (20, 21).

Functional radionuclide imaging, represented by PET-CT, complements traditional imaging modalities in identifying MTC lesions (25). [^{18}F]fluorodeoxyglucose ([^{18}F]FDG) is the most widely used diagnostic radiopharmaceutical worldwide (the only approved positron-emitting diagnostic molecule in China) and has been utilized to detect recurrent or metastatic MTC due to its association with increased glucose metabolism. However, 30% to 40% of patients with MTC with elevated calcitonin levels exhibit negative [^{18}F]FDG PET-CT findings (12, 26), and false positive may occur owing to the elevated glucose consumption in inflammatory conditions (27). Subsequently, [^{18}F]fluorodihydroxyphenylalanine ([^{18}F]FDOPA) and [^{68}Ga]Ga-somatostatin analogs ([^{68}Ga]Ga-SSA) have been investigated and reported to exhibit high specificity (25); however, their accessibility and the sensitivity for detecting MTC require further improvement (12, 13, 28, 29). For postoperative patients with a persistently elevated serum calcitonin level (which may or may not exceed a threshold of 150 pg/mL), the National Comprehensive Cancer Network guidelines favor [^{18}F]FDG or [^{68}Ga]Ga-SSA PET-CT when traditional imaging is negative (30), and the European Association of Nuclear Medicine guidelines suggest [^{18}F]FDOPA or [^{18}F]FDG PET-CT to localize the potential residual lesions (25). Nonetheless, a novel radiopharmaceutical with sufficient MTC detection and diagnostic accuracy has yet to be developed.

Fibroblast activation protein inhibitor (FAPI) is a small-molecule radiopharmaceutical targeting the overexpressed FAP in cancer-associated fibroblasts (31) and has emerged as a complementary or alternative tool for other imaging modalities due to its high and selective tumor uptake across multiple cancers (32). Given the excellent colocalization of MTC and FAP (expressed in tumor stroma; ref. 33), [^{68}Ga]Ga-FAPI PET-CT has been shown to detect additional metastatic MTC lesions that were missed by standard imaging in case reports (34, 35). A recent retrospective study suggested that [^{68}Ga]Ga-FAPI PET-CT outperformed [^{68}Ga]Ga-SSA PET-CT in identifying lung, liver, bone, and pleural metastases of MTC (36); however, many of these studies did not utilize gold-standard histopathology for validation. Furthermore, current FAPIs exhibit a short blood half-life and limited tumor retention (restricted to a few hours), and the diagnostic performance as well as the therapeutic potentiality can be further improved (37).

We have previously reported a platform technology by adding a sulfur (VI)-fluoride exchange (SuFEx) chemistry-based linker to radiopharmaceuticals for tumor-selective covalent ligation (38). When this SuFEx-engineered covalent targeted radioligand (CTR) is integrated into FAPI, the molecule achieves more than 80% covalent binding to the tyrosine residue of FAP, with minimal dissociation for up to 6 days (38). In two patients with MTC, the ^{68}Ga-labeled CTR-FAPI ([^{68}Ga]Ga-CTR-FAPI) PET-CT identified more lesions (n = 8 vs. 4) and exhibited higher tumor uptake [maximum standardized uptake value (SUV_{max}) = 12.68 ± 7.63 vs. 7.90 ± 5.69] compared with the original FAPI (38), facilitating tumor detection by the significantly improved tumor retention. The irreversible covalent ligation also facilitated targeted radionuclide therapy, in which CTR-FAPI carrying therapeutic β- and α-radionuclide resulted in a nearly complete regression of implanted tumor grafts in animal models, providing a promising solution to MTC management from both diagnostic and therapeutic perspectives.

The current study was a first-in-class clinical trial of CTR, prospectively conducting a head-to-head comparison between [^{68}Ga]Ga-CTR-FAPI PET-CT and the currently approved [^{18}F]FDG PET-CT in patients with MTC, with the primary objective to evaluate their patient-based detection rates. Quantitative parameters of [^{68}Ga]Ga-CTR-FAPI PET-CT and [^{18}F]FDG PET-CT were also compared in each individual lesion to interpret the findings on detection rates. The diagnostic accuracy, for the first time, was validated on lesions that allowed for point-to-point matching of PET-CT images and histopathology. Treatment plans and their modifications according to [^{68}Ga]Ga-CTR-FAPI PET-CT were also documented to reflect the real-world impact of the CTR. This study aims to provide a new standard of imaging with sufficient diagnostic accuracy to facilitate precision management for patients with MTC.

RESULTS

Study Design and Baseline Characteristics

This study was a prospective, single-center, open-labeled, single-arm comparative clinical trial designed to assess the effectiveness of [^{68}Ga]Ga-CTR-FAPI PET-CT compared with the currently approved [^{18}F]FDG PET-CT in the evaluation of patients with MTC. Patients with newly diagnosed, recurrent, or metastatic MTC with biochemical residual disease (serum calcitonin >10 pg/mL) and no prior or ongoing targeted therapy were enrolled between May 11, 2023, and February 1, 2024. The [^{68}Ga]Ga-CTR-FAPI PET-CT, [^{18}F]FDG PET-CT, and serum calcitonin level assessments were performed on separate days.

A total of 158 patients were assessed for eligibility, with 62 patients signing informed consent to undergo [^{68}Ga]Ga-CTR-FAPI PET-CT, and 50 patients finally enrolled in the current analysis (Fig. 1A). Eight patients were newly diagnosed with MTC, whereas forty-two patients had persistent disease. The median calcitonin level was 885 (IQR, 365–1911) for the whole population, 606 (IQR, 388–930) for newly diagnosed patients with MTC, and 974 (IQR, 355–2,061) for those with persistent disease. Forty-six patients received the two PET-CT scans with a time interval of 1 day, whereas four patients received the two PET-CT scans with a time interval larger than 1 day (range, 2–22 days). No strict order between [^{68}Ga]Ga-CTR-FAPI PET-CT and [^{18}F]FDG PET-CT scans was required, with 43 patients receiving [^{18}F]FDG PET-CT before [^{68}Ga]Ga-CTR-FAPI PET-CT and seven patients receiving

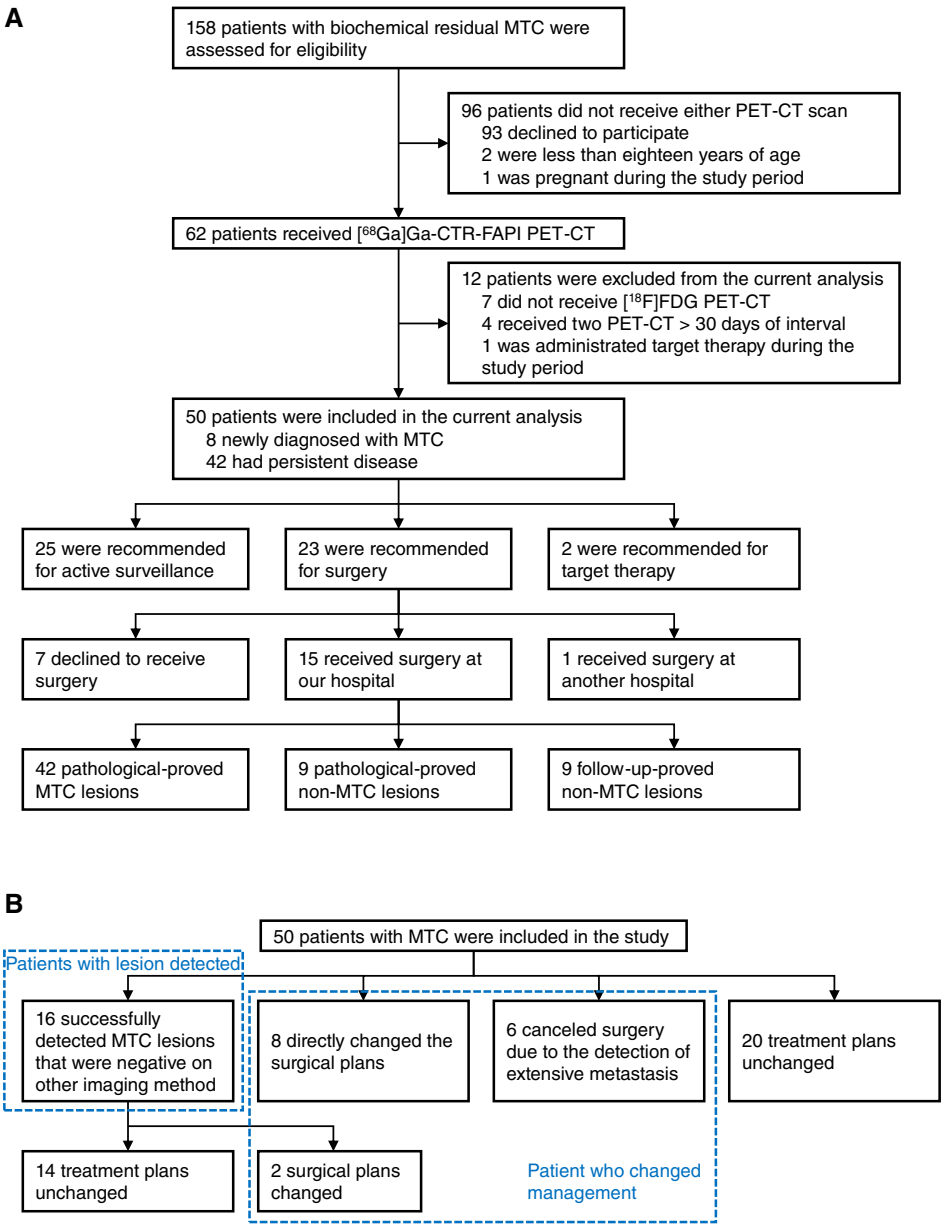

Figure 1. Study profile. A total of 50 patients were included in the study, and 60 lesions from 15 patients who received surgery were applied to validate the accuracy of the PET-CTs in identifying MTC lesions (**A**). Impact of [^{68}Ga]Ga-CTR-FAPI PET-CT on clinical practice, with 32% (16/50) patients changing management following [^{68}Ga]Ga-CTR-FAPI PET-CT (**B**).

[^{18}F]FDG PET-CT after [^{68}Ga]Ga-CTR-FAPI PET-CT. Baseline characteristics of the study population are outlined in Supplementary Table S1.

Superior Detection Rate of [^{68}Ga]Ga-CTR-FAPI PET-CT Facilitated MTC Evaluation

The [^{68}Ga]Ga-CTR-FAPI PET-CT scans were evaluated independently by three nuclear medicine physicians, and the [^{18}F]FDG PET-CT scans were assessed by another three nuclear medicine physicians. All of the readers were blinded to patient information and were masked to the interpretation of other readers and other imaging modalities.

The primary objective of the study was accomplished: The patient-based detection rate for [^{68}Ga]Ga-CTR-FAPI was higher than that for [^{18}F]FDG PET-CT (98% vs. 66%; P = 0.0002; Fig. 1B). Improvements in detection rates with [^{68}Ga]Ga-CTR-FAPI PET-CT were also observed across various anatomical regions, including a 22% increase in the head and neck regions, a 16% increase in the thoracic region, a 18% increase in the abdomen region, and a 38% increase in the skeletal system (Table 1; Supplementary Fig. S1). The better detection by [^{68}Ga]Ga-CTR-FAPI was not restricted to certain subpopulations, as similar trends were noted when stratified by calcitonin levels; however, the difference did not reach

Table 1. Patient-based and region-based detection rate of [^{68}Ga]Ga-CTR-FAPI and [^{18}F]FDG.

	[^{18}F]FDG	[^{68}Ga]Ga-CTR-FAPI	*P* value
Detection rate in the whole body	0.66 (0.51–0.79)	0.98 (0.93–1.00)	0.0002
Detection rate in the head and neck region	0.50 (0.36–0.64)	0.72 (0.58–0.84)	0.0098
Detection rate in the thoracic region	0.34 (0.21–0.49)	0.50 (0.36–0.64)	0.0269
Detection rate in the abdomen region	0.10 (0.03–0.22)	0.28 (0.16–0.43)	0.0077
Detection rate in the skeleton	0.16 (0.07–0.29)	0.54 (0.39–0.68)	<0.0001

Data are presented as patient-based and region-based detection rates with a 95% confidence interval.

statistical significance due to the small number of patients in the subgroups (Supplementary Tables S2–S4). Inter-reader agreements at each region for both imaging modalities were good, with Fleiss Kappa performances ranging from 0.643 to 1.000 for [^{18}F]FDG PET-CT and 0.733 to 0.947 for [^{68}Ga]Ga-CTR-FAPI PET-CT (Supplementary Table S5), indicating the reproducibility of the manual reading results.

Higher Tumor Uptake of [^{68}Ga]Ga-CTR-FAPI Attributed to Better Detection of MTC

A quantitative analysis was conducted to elucidate the enhanced detection of MTC. [^{68}Ga]Ga-CTR-FAPI PET-CT identified a total of 643 lesions from the 50 patients, with a median number of four (IQR, 2–11) lesions per patient. In comparison, [^{18}F]FDG PET-CT only recognized 190 lesions (29.5% of [^{68}Ga]Ga-CTR-FAPI PET-CT identified lesions), with a median number of two (IQR, 0–4) lesions per patient. For the lesions that were avid on either PET-CT, the lesion uptake of [^{68}Ga]Ga-CTR-FAPI was higher than that of [^{18}F]FDG PET-CT, with a SUV_{max} of 11.71 ± 9.16 compared with 2.55 ± 1.73 ($P < 0.0001$) and a tumor-to-normal (T/N) ratio of 6.20 ± 5.52 versus 1.51 ± 1.12 ($P < 0.0001$; Table 2; Supplementary Fig. S2A–S2C). The lesion uptake of [^{68}Ga]Ga-CTR-FAPI remained higher than that of [^{18}F]FDG in lesions that were avid on both imaging modalities (Supplementary Table S6), stratified by anatomical locations (Table 2), calcitonin levels (Supplementary Table S7), carcinoembryonic antigen (CEA) levels (Supplementary Table S8), and whether the disease was newly diagnosed or persistent (Supplementary Table S9), implying the superior tumor uptake was not limited to certain subpopulations. Examples of [^{18}F]FDG PET-CT and [^{68}Ga]Ga-CTR-FAPI PET-CT in metastatic MTC are illustrated in Fig. 2A–D.

Better Diagnostic Accuracy in Surgically Validated Lesions

The validation of imaging findings with gold-standard histopathology is crucial for translating a novel radiopharmaceutical into clinical practice. However, previous imaging reports primarily focused on comparisons between imaging modalities and lacked an exploration of diagnostic accuracy. In the current study, lesions suspected to be malignant in at least one imaging modality (including [^{68}Ga]Ga-CTR-FAPI PET-CT, [^{18}F]FDG PET-CT, contrast-enhanced CT, or ultrasound) were separately identified and labeled to evaluate the diagnostic accuracy of these imaging techniques.

Among the enrolled patients, 16 underwent surgery, with 15 receiving surgery at our hospital, and a point-to-point matching of PET-CT images with histopathology was performed. One patient received surgery at another institute in which the matching of PET-CT images with the surgical specimen was unfeasible. The median interval between surgery and the latest PET-CT scan was 9 days (IQR, 6–18). A total of 60 lesions were considered malignant on at least one imaging modality and were definitive for lesion property, with 44, 38, 35, and 32 lesions suspected to be malignant on [^{68}Ga]Ga-CTR-FAPI PET-CT, [^{18}F]FDG PET-CT, contrast-enhanced CT, and ultrasound, respectively (Supplementary Table S10). For the gold-standard reference of the 60 lesions, 42 were pathologically confirmed as MTC lesions, 9 were pathologically confirmed as non-MTC lesions, and 9 were non-MTC lesions confirmed by follow-up (lesions were not resected, and serum calcitonin levels returned to normal 1 month after surgery, suggesting that the nonresected lesions were benign; Fig. 1A).

The [^{68}Ga]Ga-CTR-FAPI PET-CT exhibited higher diagnostic accuracy for identifying MTC lesions compared with the [^{18}F]FDG PET-CT (96.7% vs. 43.3%; $P < 0.0001$; Table 3, examples shown in Fig. 3A–D) and also outperformed the ultrasound combined with contrast-enhanced CT (96.7% vs. 66.7%; $P = 0.0003$; Supplementary Table S11). In the *post hoc* quantitative imaging analysis, MTC lesions exhibited higher uptake than non-MTC lesions in [^{68}Ga]Ga-CTR-FAPI PET-CT, with a SUV_{max} of 14.54 ± 11.11 compared with 2.35 ± 1.63 ($P < 0.0001$); however, no differences existed in the [^{18}F]FDG uptake between MTC and non-MTC lesions (Table 4). In the *post hoc* pathologic analysis, MTC colocalized with FAP expression in the tumor stroma (Supplementary Fig. S3A–S3C), and a linear correlation between [^{68}Ga]Ga-CTR-FAPI uptake (SUV_{max} and SUV_{mean}) and FAP expression was observed ($r^2 = 0.793$ and 0.843, respectively; Supplementary Fig. S3D and S3E).

Change of Surgical Plans and Satisfactory Outcomes in Patients with MTC

Thanks to the sufficient detection rate and diagnostic accuracy, [^{68}Ga]Ga-CTR-FAPI PET-CT was capable of changing the surgical plan of MTC because the current surgical extent of MTC (traditional imaging–based surgery or calcitonin-based surgery) was inaccurate.

Among the 15 patients who received surgery locally, 6 newly diagnosed MTC achieved R0 resection (complete resection of all [^{68}Ga]Ga-CTR-FAPI PET-CT-avid lesions), 1 with newly

Table 2. Comparison between [^{68}Ga]Ga-CTR-FAPI and [^{18}F]FDG in suspected malignant lesions.

	[^{18}F]FDG	[^{68}Ga]Ga-CTR-FAPI	*P* value
Whole body			
SUV_{max}	2.55 ± 1.73	11.71 ± 9.16	<0.0001
SUV_{mean}	1.79 ± 0.84	6.57 ± 2.82	<0.0001
T/N ratio	1.51 ± 1.12	6.20 ± 5.52	<0.0001
Head neck			
SUV_{max}	3.02 ± 2.24	11.50 ± 9.23	<0.0001
SUV_{mean}	2.08 ± 1.25	6.56 ± 3.49	<0.0001
T/N ratio	2.14 ± 1.53	7.55 ± 6.04	<0.0001
Thorax			
SUV_{max}	2.57 ± 1.96	9.74 ± 7.23	<0.0001
SUV_{mean}	1.72 ± 0.89	5.94 ± 2.53	<0.0001
T/N ratio	1.96 ± 1.44	7.06 ± 5.67	<0.0001
Abdomen			
SUV_{max}	2.45 ± 0.94	9.22 ± 7.39	<0.0001
SUV_{mean}	1.97 ± 0.53	5.81 ± 2.24	<0.0001
T/N ratio	1.03 ± 0.37	3.57 ± 2.26	<0.0001
Skeleton			
SUV_{max}	2.40 ± 1.70	13.60 ± 9.99	<0.0001
SUV_{mean}	1.59 ± 0.66	7.13 ± 2.73	<0.0001
T/N ratio	1.38 ± 0.90	6.75 ± 5.99	<0.0001

Data are presented as the mean ± SD of each variable.

diagnosed MTC achieved R1 resection, and one with newly diagnosed MTC was unable to resect all [^{68}Ga]Ga-CTR-FAPI PET-CT–avid lesions (distant metastasis existed). Among the seven patients with persistent MTC who received surgery locally, two achieved R0 resection whereas five could not remove all [^{68}Ga]Ga-CTR-FAPI PET-CT–avid lesions.

All six patients with newly diagnosed MTC who achieved R0 resection reached biochemical cure 1 month after surgery (the strictest curative level for MTC, indicating no residual tumor existed), with a 1-month postsurgery calcitonin level of 2.72 ± 1.83 pg/mL and a postsurgery to presurgery calcitonin ratio of 0.54% ± 0.42% (Supplementary Table S12). A total of 83.3% (5/6) of the surgical plans were changed as per calcitonin level–based surgery (eliminating the need for prophylactic lateral neck dissection), and 33.3% (2/6) of the surgical plan was modified compared with traditional imaging–based surgery (one patient necessitated additional neck dissection and one patient avoided neck dissection). The patient with newly diagnosed MTC with R1 resection and the two patients with persistent MTC with R0 resection also experienced favorable outcomes, with 1-month postsurgery calcitonin levels of 19.1 and 27.4 ± 24.9 pg/mL, respectively (Supplementary Table S12). The surgical plans for both patients with persistent MTC were modified as [^{68}Ga]Ga-CTR-FAPI PET-CT detected additional malignant lesions not visible on traditional imaging, necessitating more extensive surgery. In contrast, six patients were unable to have all [^{68}Ga]Ga-CTR-FAPI PET-CT–avid lesions removed (already known during surgery), with a 1-month postsurgery to presurgery calcitonin ratio of 59.2% ± 35.5% (Supplementary Table S12). A total of 33.3% (2/6) of the surgical plan was enlarged compared with traditional imaging–based surgery.

In comparison, of the 15 patients who received surgery, 3 would have canceled surgery due to the inability to locate lesions using [^{18}F]FDG PET-CT, and one patient would have altered surgical plan according to [^{18}F]FDG PET-CT, resulting in an uncured disease.

Real-World Impact of [^{68}Ga]Ga-CTR-FAPI PET-CT in Patient Management

Initial treatment plans and their modifications following [^{68}Ga]Ga-CTR-FAPI PET-CT were collected from the referring physicians to assess the real-world impact of the CTR (Fig. 1B). In addition to the 32% (16/50) patients able to identify MTC lesions that were negative on traditional imaging, a total of 20% (10/50) patients modified their surgical plans, and 12% (6/50) patients initially scheduled for surgery transitioned to active surveillance or targeted therapy due to the detection of extensive distant metastasis or unresectable lesions.

Safety

There was no grade 2 or higher adverse event. Nonspecific grade 1 events were noted in 2 of the 50 patients (4%) after [^{18}F]FDG PET-CT and 1 of the 50% patients (2%) following [^{68}Ga]Ga-CTR-FAPI PET-CT (Supplementary Table S13). None of the events necessitated further intervention, and no patient discontinued the study due to the adverse events.

DISCUSSION

In this first-in-class clinical trial of CTR, [^{68}Ga]Ga-CTR-FAPI PET-CT demonstrated a superior detection rate, tumor uptake, and diagnostic accuracy in patients with MTC compared with [^{18}F]FDG PET-CT. The primary endpoint was met: the detection rate for [^{68}Ga]Ga-CTR-FAPI PET-CT was higher than that for [^{18}F]FDG PET-CT in patients with MTC (98% vs. 66%). This finding can be further supported by the higher lesion uptake (SUV_{max} = 11.71 ± 9.16) and diagnostic accuracy (96.7%) of [^{68}Ga]Ga-CTR-FAPI PET-CT, all of which contribute to the precision diagnosis of MTC. Additionally, 32% patients had management changes following [^{68}Ga]Ga-CTR-FAPI PET-CT, and 66.7% patients changed surgical plans, transforming precision diagnosis into precision management.

Localizing MTC lesions is crucial for both initial diagnosis and follow-up, as the location and distribution of disease directly influence the therapeutic strategies. However, [^{18}F]FDG, [^{18}F]FDOPA, and [^{68}Ga]Ga-SSA reported detection rates of 59% to 71% per patient (12, 13), and in 16% to 28% of patients no lesion was able to be located despite the use of multiple imaging techniques (16–19). [^{18}F]FDG was chosen as the comparison because it is the only approved positron-emitting diagnostic molecule in multiple countries and was supported by both National Comprehensive Cancer Network and European Association of Nuclear Medicine guidelines (25, 30). Given the colocalization of MTC and FAP, along with the positive correlation between FAP expression and FAPI uptake (39), targeting elevated FAP expression in tumor stroma presents an alternative solution. In our study, [^{68}Ga]Ga-CTR-FAPI PET-CT achieved a patient-based detection rate of 98%, identifying 3.4

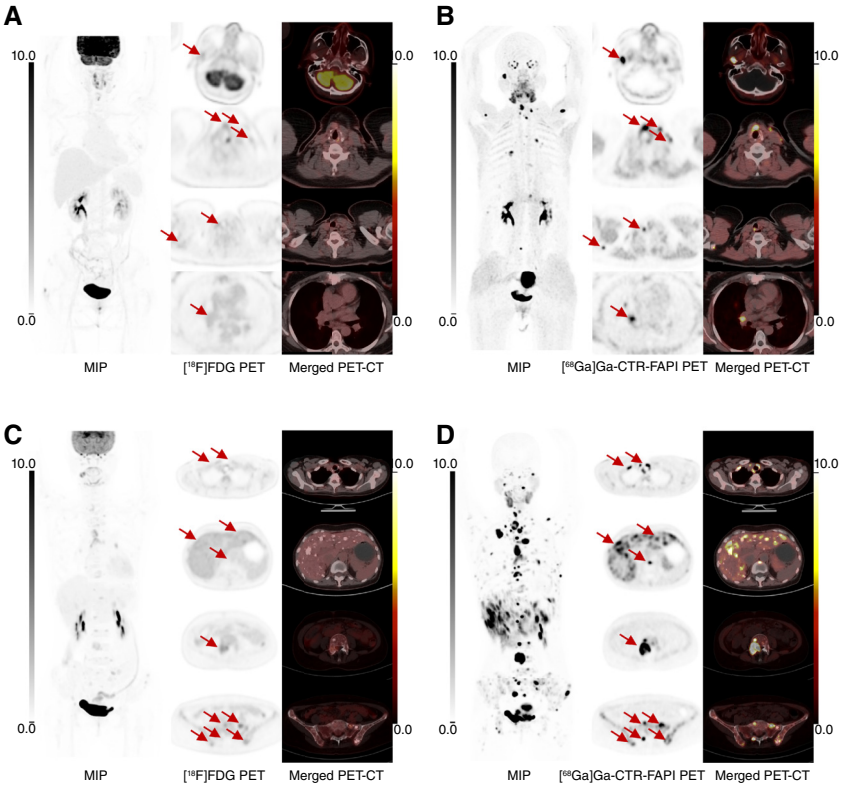

Figure 2. Examples of [^{18}F]FDG PET-CT and [^{68}Ga]Ga-CTR-FAPI PET-CT in patients with MTC. A 47-year-old female who had previously received thyroidectomy, bilateral neck dissection, and upper mediastinum lymph node dissection currently had a calcitonin level of 1,772 pg/mL. Despite [^{18}F]FDG PET-CT yielding negative results for MTC lesions (**A**), [^{68}Ga]Ga-CTR-FAPI PET-CT detected malignant lesions in the head and neck (including the thyroid bed and neck lymph node), thoracic lymph nodes, and skeleton (involving the skull, thoracic bone, and lumbar vertebra, which can be seen through both maximum intensity projection (MIP) and cross-sectional images; **B**), with a SUV_{max} of 3.83–22.37 and a T/N ratio of 3.28–14.28. Similarly, a 58-year-old female who had undergone thyroidectomy and lymph node dissection currently had a calcitonin level of 140,983 pg/mL. Whereas [^{18}F]FDG PET-CT was able to identify several metastatic lesions (**C**), [^{68}Ga]Ga-CTR-FAPI PET-CT identified extensive whole-body metastasis (**D**) with a SUV_{max} of 4.19–49.73 and a T/N ratio of 2.76–12.97.

times the number of lesions than [^{18}F]FDG PET-CT and exhibiting 4.1 times of the T/N ratio than that of [^{18}F]FDG PET-CT. In a previous retrospective study, [^{68}Ga]Ga-DOTA.SA.FAPI (a noncovalent FAPI) outperformed [^{68}Ga]Ga-DOTANOC (a type of [^{68}Ga]Ga-SSA) in patients with MTC thanks to the clearer background in the abdomen and bone (36). These results suggest that FAPI PET-CT has the potentiality to locate MTC lesions more effectively than current methods.

The diagnostic and therapeutic efficacy of radiopharmaceuticals has long been restricted by the challenges of achieving sustainable tumor targeting and rapid clearance from healthy tissue simultaneously. The original FAPI interacts reversibly with its ligand with an *in vivo* half-life restricted to a few hours, thereby missing small malignant lesions due to insufficient tumor-to-background activity. In contrast, our targeted covalent strategy created covalent bonds between ligands and small-molecule radiopharmaceuticals, allowing the identification of more lesions that were neglected in the original FAPI PET-CT (supported by histopathology; ref. 38). The current study was the first-in-class clinical trial of CTR, not only providing valuable verification of this strategy to reformulate the design of radiopharmaceutical but also furnishing, to the best of our knowledge, the most appropriate radiopharmaceutical for MTC. It should be noted that

Table 3. Accuracy of [^{68}Ga]Ga-CTR-FAPI and [^{18}F]FDG in identifying MTC or non-MTC lesions.

	[^{18}F]FDG	[^{68}Ga]Ga-CTR-FAPI	*P* value
Accuracy	43.3% (30.6%–56.8%)	96.7% (88.5%–99.6%)	<0.0001
Sensitivity	54.8% (38.7%–70.2%)	100.0% (91.6%–100.0%)	<0.0001
Specificity	16.7% (3.6%–41.4%)	88.9% (65.3%–98.6%)	0.0019

Data are presented as the mean ± SD of each variable.

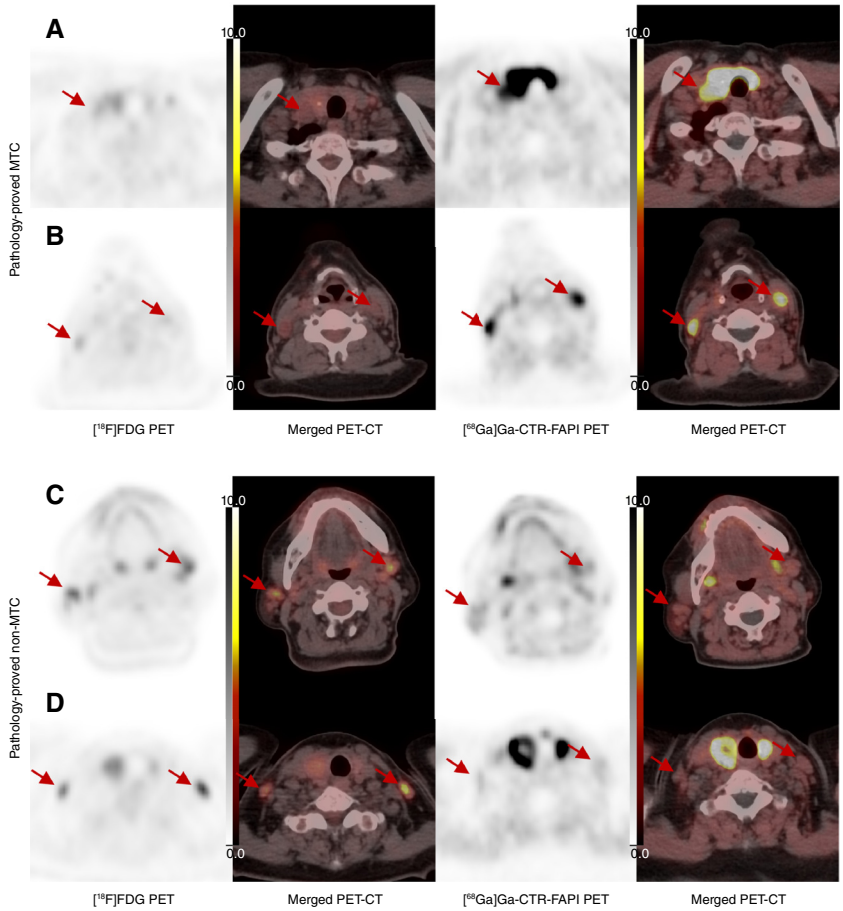

Figure 3. Examples of [^{18}F]FDG PET-CT and [^{68}Ga]Ga-CTR-FAPI PET-CT in pathologically proven MTC and non-MTC lesions. A 66-year-old female, newly diagnosed with MTC, had a current calcitonin level of 4,180 pg/mL. The right neck level VI lymph node (**A**) and the bilateral level III lymph node (**B**) exhibited moderate [^{18}F]FDG uptake (SUV_{max} = 2.81–3.69 and T/N ratio 1.78–2.34) but showed significant [^{68}Ga]Ga-CTR-FAPI uptake (SUV_{max} = 10.34–13.17 and T/N ratio 6.47–8.24), and postsurgical histopathology confirmed the lesions to be metastatic lymph nodes. Conversely, the bilateral level II lymph node (**C**) and level V lymph node (**D**) displayed significant [^{18}F]FDG uptake (SUV_{max} = 5.14–7.98, T/N ratio 3.26–5.06) but only mild [^{68}Ga]Ga-CTR-FAPI uptake (SUV_{max} = 2.52–3.90, T/N ratio 1.57–2.44), and histopathology indicated that the lesions were not lymph nodes with MTC metastasis. Furthermore, the [^{68}Ga]Ga-CTR-FAPI PET-CT excluded distant metastasis of MTC, and the patient reached biochemical cure (1-month postsurgical calcitonin of 1.49), suggesting that no residual MTC cells remained.

CTR-FAPI is a pan-cancer radiopharmaceutical that can be expanded to a broad range of indications, and the application of CTR-FAPI in other tumors is also anticipated.

In addition to the visual and quantitative assessments, the reliability of [^{68}Ga]Ga-CTR-FAPI PET-CT in identifying MTC was validated through histopathology/calcitonin-based follow-up of 60 lesions. This point-to-point matching of PET-CTs and the gold-standard reference was essential for establishing the diagnostic accuracy of this novel radiopharmaceutical. [^{68}Ga]Ga-CTR-FAPI PET-CT exhibited higher accuracy (96.4%) in identifying MTC than [^{18}F]FDG PET-CT and traditional imaging, thereby proving the reliability of [^{68}Ga]Ga-CTR-FAPI PET-CT. Future translational studies are necessary to elucidate the mechanism of FAP-based MTC detection (40–46).

Table 4. Uptake comparison of [^{68}Ga]Ga-CTR-FAPI and [^{18}F]FDG in MTC and non-MTC lesions.

	[^{18}F]FDG			[^{68}Ga]Ga-CTR-FAPI		
	MTC (n = 42)	Non-MTC (n = 18)	P value	MTC (n = 42)	Non-MTC (n = 18)	P value
SUV_{max}	3.56 ± 2.56	3.93 ± 2.89	0.623	14.54 ± 11.11	2.35 ± 1.63	<0.0001
SUV_{mean}	2.43 ± 1.34	2.84 ± 1.82	0.325	7.83 ± 4.23	1.87 ± 1.25	<0.0001
T/N ratio	2.36 ± 1.77	2.57 ± 1.63	0.679	8.16 ± 7.37	1.51 ± 0.91	<0.0001

Data are presented as the mean ± SD of each variable.

Thanks to its sufficient detection rate and diagnostic accuracy, [^{68}Ga]Ga-CTR-FAPI PET-CT facilitated precision surgery of MTC, as there remains no consensus on the surgical extent of MTC (some physicians rely on preoperative ultrasound and do not perform prophylactic lateral neck dissection if the ultrasound is negative, whereas others advocate prophylactic lateral neck dissection according to serum calcitonin level; refs. 6, 7). In our study, five patients with newly diagnosed MTC were spared from prophylactic lateral neck dissection because the [^{68}Ga]Ga-CTR-FAPI PET-CT results were negative for the lateral neck. All of these patients reached biochemical cure 1 month after surgery, suggesting that no remaining tumor existed. On the other hand, five patients with MTC had additional malignant lesions detected by [^{68}Ga]Ga-CTR-FAPI PET-CT, and the excision of [^{68}Ga]Ga-CTR-FAPI PET-CT–avid lesions yielded positive pathologic outcomes. Inspired by the promising results, a prospective interventional clinical trial (NCT06277180) was recently launched to investigate the potential of [^{68}Ga]Ga-CTR-FAPI PET-CT to guide the surgical extent of MTC. However, it is essential to note that although excision of [^{68}Ga]Ga-CTR-FAPI PET-CT–avid lesions is important, standard dissection of regional lymph nodes should be performed to address the possible minimum metastases in small lymph nodes, aligning with the surgical principles for all types of thyroid cancers.

The region-based detection rate, along with the calcitonin-stratified detection, deepened our understanding of the disease. Generally, patients with higher calcitonin levels experienced a greater burden of disease. In addition to the head and neck region, thoracic lymph nodes were the second common site for MTC involvement; however, not only the upper mediastinum but also the anterior and middle mediastinum areas may be affected, and small lesions that did not satisfy the RECIST criteria can still be malignant and warrant intervention (47). Whereas liver metastasis presented predominantly in patients with calcitonin levels higher than 500 pg/mL, bone metastasis can occur across any calcitonin levels, reshaping the previous opinion that distant metastasis only occurs when calcitonin levels surpass 1,000 pg/mL (8). In contrast to differentiated thyroid carcinoma, the lung was not the primary site for MTC metastasis and was observed in only 4% of patients. Nevertheless, the subgroup analyses in the current study were performed to confirm that the improved detection and tumor uptake were not confined to specific subpopulations, and the findings warranted exploration in larger patient populations.

Significant changes in the management of patients with MTC shall occur when [^{68}Ga]Ga-CTR-FAPI PET-CT is integrated into clinical practice: (i) detection of the MTC lesion, including in postsurgery patients with elevated calcitonin levels who are negative, inconclusive, or incompletely assessed by traditional imaging, as well as presurgery patients, to exclude distant metastasis; (ii) changes to the surgical plan, where additional malignant lesions may be resected and prophylactic neck dissection may be avoided; and (iii) determination of the screening and follow-up schedules, prioritizing lesion-located regions. However, a major limitation of this study was the inability to correlate [^{68}Ga]Ga-CTR-FAPI PET-CT direct therapy with improvements in patient survival, particularly as patients with unresectable disease lack efficient treatment options. Additional limitations include the relatively small patient cohort in this explorative trial, the difficulty in recruiting patients with very low calcitonin levels, and the inability to histopathologically validate the PET-CT findings in the abdomen region and bone. For future works, CTR-FAPI carrying therapeutic radionuclide (e.g., ^{177}Lu) necessitates attentive investigations, which have shown considerable improvements over unmodified FAPIs in preclinical models (38).

In conclusion, [^{68}Ga]Ga-CTR-FAPI PET-CT demonstrated a superior detection rate, tumor uptake, and diagnostic accuracy compared with [^{18}F]FDG PET-CT in patients with MTC, facilitating precision diagnosis and management of the disease. Together with previous reports indicating that [^{68}Ga]Ga-CTR-FAPI outperforms the original FAPI, [^{68}Ga]Ga-CTR-FAPI PET-CT has the potential to become the standard of imaging for patients with MTC.

METHODS

Study Design and Participants

This study was a prospective, single-center, open-labeled, single-arm comparative imaging trial designed to assess the effectiveness of [^{68}Ga]Ga-CTR-FAPI PET-CT compared with the currently approved [^{18}F]FDG PET-CT in evaluating patients with MTC. The study belonged to an independent subcohort of an investigator-initiated trial exploring the clinical value of [^{68}Ga]Ga-CTR-FAPI PET-CT in malignant tumors (NCT06084767), which was approved by the Institutional Review Board (2023YJZ20). Written informed consent was obtained from all study participants. The Clinical Protocol and Notification to Attending Physicians are included as supplementary data. Supplementary Table S14 provides information about the representativeness of the study population in relation to the larger population.

Inclusion criteria for the current study were as follows: (i) age between 18 and 75 years; (ii) newly diagnosed MTC or recurrent or metastatic MTC with biochemical persistent disease (serum calcitonin >10 pg/mL); (iii) no previous or currently administrated targeted therapy (i.e., vandetanib and cabozantinib; refs. 24, 48, 49), as targeted therapy can significantly affect the calcitonin levels in MTC; (iv) no significant abnormalities in blood routine, liver function, and kidney function or recent onset of infections; amd (v) willingness to participate and ability to sign the informed consent form. For patients with persistent MTC, those exhibiting negative findings on traditional imaging or discordant results between traditional imaging and calcitonin levels were encouraged to enroll as the PET-CTs might provide additional benefit. Patients with stable calcitonin levels or definitive findings on traditional imaging were discouraged from participation.

Based on previous meta-analyses, the patient-based detection rate of [^{18}F]FDG PET-CT in patients with MTC with elevated calcitonin ranged from 59% to 69% (estimated detection rate 65%; refs. 12, 26), and the detection rate of another FAPI ([^{68}Ga]Ga-DOTA.SA.FAPI) in patients with MTC was 96% (estimated using lesion-based detection rate; ref. 36). A statistical power analysis established prospectively that enrolling at least 44 participants would provide an 80% power of the test to detect the expected differences of 31% detection rates at the patient level with two-sided α of 0.05. Considering a potential dropout rate of 10%, the final sample size was set as 50 patients.

PET-CT Imaging and Serum Calcitonin

[^{68}Ga]Ga-CTR-FAPI PET-CT, [^{18}F]FDG PET-CT, and serum calcitonin level were assessed on separate days with a maximum interval of 30 days. No strict order between [^{68}Ga]Ga-CTR-FAPI PET-CT and [^{18}F]FDG PET-CT was required, as they targeted different receptors on different cells.

Patients were required to fast for at least 4 hours prior to [^{18}F]FDG administration, whereas no specific preparation was required for [^{68}Ga]Ga-CTR-FAPI. Both [^{18}F]FDG and [^{68}Ga]Ga-CTR-FAPI were hospital-produced and administrated intravenously, with doses of 3.7 to 5.5 MBq/kg for [^{18}F]FDG and 1.8 to 3.7 MBq/kg for [^{68}Ga]Ga-CTR-FAPI, respectively. PET-CT scans were performed 60 minutes after administration using a uEXPLORER total-body PET-CT scanner (United Imaging Healthcare). The PET images were acquired with an axial field of view of 194 cm, an original matrix of 192 × 192, and a slice thickness of 3.0 mm, and the voxels were subsequently normalized by body weight and decay factor to generate a SUV map. All patients were required to receive local [^{68}Ga]Ga-CTR-FAPI PET-CT, and the DICOM images of [^{18}F]FDG PET-CT were obtained for patients who had previously received [^{18}F]FDG PET-CT at other institutes.

Safety

Patients were monitored for adverse events during and within 2 hours after radiotracer administration. Vital signs, including body temperature, heart rate, and blood pressure, were recorded before and after the injection of each radiopharmaceutical. Phone call report or outpatient visit was available for patients to report any delayed adverse event.

Manual Image Interpretation

Manual evaluation was first implemented for patient-based and region-based detection. The [^{68}Ga]Ga-CTR-FAPI PET-CT scans were evaluated independently by three nuclear medicine physicians, and the [^{18}F]FDG PET-CT scans were assessed by another three nuclear medicine physicians. All of the readers were blinded to patient information and not involved in the study's design or data collection. The readers were masked to the interpretation of the other five readers and the other imaging modalities (i.e., the physician reading [^{18}F]FDG PET-CT did not read [^{68}Ga]Ga-CTR-FAPI PET-CT). Anonymized data, including PET-CT scans, patient history, and the recent calcitonin level, were provided. Readers were required to assess the presence of MTC in the following regions: head and neck region (including the thyroid bed and neck lymph node), thoracic region (mediastinum lymph node, hilar lymph node, axillary lymph node, and lung), abdomen region (liver and retroperitoneal lymph node), and skeleton system (skull, vertebra, thoracic bone, pelvic bone, and limb). Patient-based detection of MTC was summarized from the region-based detections. In cases of disagreement between readers, a consensus was reached through a majority rule vote.

Quantitative Image Evaluation

Quantitative analysis of individual lesions was performed to interpret the findings from physician readings. Lesions identified on [^{68}Ga]Ga-CTR-FAPI PET-CT were semi-automatically segmented by an experienced nuclear medicine physician and edited by a senior surgeon and another nuclear medicine physician. A spherical reference region of interest (ROI_{ref}) with a diameter of 0.5 cm (lymph node), 1.0 cm (bone and thyroid if not resected), or 2.0 cm (lung, liver, and aorta) was manually placed on normal organs, and the maximum SUV of normal organs (N_{max}) was calculated. Lesion ROIs were first semi-automatically created for regions with a SUV greater than 2.0 × N_{max} of the corresponding normal regions and were subsequently manually revised. Areas with focal uptake that were visually higher than the surrounding background but did not reach 2.0 × N_{max} were also considered positive and delineated into an ROI. Areas with a SUV higher than 2.0 × N_{max} but were known as alternative benign or malignant tumor (i.e., adrenal pheochromocytoma) or nonmalignant lesions (i.e., history and image-diagnosed arthritis) were considered negative and excluded from the ROI. ROIs were considered as separate lesions if they were anatomically discontinuous at x, y, and z axis, otherwise they were recognized as a continuous lesion.

ROIs from [^{68}Ga]Ga-CTR-FAPI PET-CT were semi-automatically coregistered to [^{18}F]FDG PET-CT and manually relocated if necessary, allowing identical regions to be analyzed across different imaging modalities. This was essential for an accurate quantification of [^{18}F]FDG PET-CT, as relying solely on delineations from [^{18}F]FDG PET-CT would significantly underestimate the disease burden. Potential malignant lesions identified on [^{18}F]FDG PET-CT were also segmented and coregistered to [^{68}Ga]Ga-CTR-FAPI PET-CT.

Treatment Decision and Surgical Validation

The treatment decision for each patient (surgery, active surveillance, or targeted therapy) was ultimately determined by the referring physician based on all available information (patient history, PET-CT results, conventional imaging findings, and calcitonin level and trends) and the patient's will. A survey was required from the referring physician to report the initial suggested treatment (before PET-CTs), the final suggested treatment (after PET-CTs), the final implemented treatment, and whether [^{68}Ga]Ga-CTR-FAPI PET-CT results influenced the treatment plan. For patients scheduled for surgery, contrast-enhanced CT and neck ultrasound were also performed.

Lesions that met the following criteria were separately obtained and labeled to evaluate the diagnostic accuracy of the imaging modalities (50, 51): (i) suspected to be malignant on least on one imaging modality ([^{68}Ga]Ga-CTR-FAPI PET-CT, [^{18}F]FDG PET-CT, contrast-enhanced CT, or ultrasound) and (ii) available for the gold-standard reference, determined by either histopathology (MTC or non-MTC) or follow-up (only to identify non-MTC lesions that were not resected and for which biochemical cure was achieved after surgery). Lesions under the following circumstances were not included: (i) considered malignant only by imaging but lacking gold-standard pathology (i.e., for patients who did not receive surgery) and (ii) considered benign by all imaging modalities, as they could not be separately labeled and point-to-point matched between imaging and intraoperative findings.

The extent of surgery was determined by the referring physician and aligned with patient preferences. Consistent with the surgical principles for all thyroid cancers (7, 52), therapeutic dissection of the relevant lymph node regions should be performed, if planned, rather than merely removing the malignant lesion. Calcitonin levels at 1 month after surgery were tested and compared with presurgery calcitonin levels to evaluate treatment response.

IHC and Pathologic Analysis

The FAP expression was determined by the IHC of FAP, and MTC was identified by the IHC of calcitonin and CEA. FAP quantification was performed semi-automatically on scanned digital slices and analyzed in high-power fields (10 × 10) containing tumor cell clusters to calculate the average optical density.

Outcomes

The primary outcome was the patient-based detection rate of [^{68}Ga]Ga-CTR-FAPI PET-CT and [^{18}F]FDG PET-CT in patients with MTC, defined as the ratio of reader-identified PET-CT–positive patients to the number of all patients (50, 53). The secondary outcomes included the following: (i) region-based detection rates (ratio of PET-CT–positive regions to the number of all patients); (ii) the value comparison of tumor uptake between [^{18}F]FDG and [^{68}Ga]Ga-CTR-FAPI PET-CT at the individual lesion level, (iii) the accuracy of the imaging modalities in identifying histopathology or calcitonin-based follow-up–confirmed MTC or non-MTC lesions; and (iv) the safety of the PET-CT reagents.

Statistical Analysis

To compare the reader-reported patient-based and region-based detection rate, the two-sided McNemar test was used to calculate the statistical differences for paired variables, and the Clopper–Pearson

test was conducted to calculate the 95% confidence interval of detection rates. Fleiss multirater Kappa statistics were utilized to assess inter-reader agreement between reviewers.

To quantify the [^{18}F]FDG and [^{68}Ga]Ga-CTR-FAPI uptake of lesions, PET parameters, including SUV_{max} (maximum SUV within the ROI), SUV_{mean} (mean SUV within the ROI), and T/N ratio (ratio of lesion SUV_{max} to the corresponding regional N_{max}), were calculated for each individual lesion (54). The mean and SD were calculated for the PET parameters and were compared using the paired sample *t* test.

To evaluate the accuracy of [^{18}F]FDG, [^{68}Ga]Ga-CTR-FAPI PET-CT, and traditional imaging (ultrasound plus contrast-enhanced CT) in identifying MTC, a lesion-based comparison between imaging identification and the gold-standard reference was performed in patients who received surgery (50, 51). Individual lesions were calculated for PET parameters (SUV_{max}, SUV_{mean}, and T/N ratio), and the gold-standard reference was determined by either histopathology (MTC or non-MTC) or follow-up (only to identify the non-MTC lesions that were not resected, and the biochemical cure was reached after surgery). The two-sided McNemar test and Clopper–Pearson test were applied to calculate the statistical differences and 95% confidence intervals. The mean and SD for the PET parameters were calculated and compared using the independent sample *t* test. To assess the treatment response after surgery, the calcitonin levels at 1 month after surgery was measured, and the ratio of 1-month postsurgical calcitonin to presurgical calcitonin were calculated. The [^{68}Ga]Ga-CTR-FAPI parameters (SUV_{max} and SUV_{mean}) and FAP expression (average optical density of IHC) were fitted into linear curves, and the coefficient of determination (r^2) was subsequently calculated.

The [^{18}F]FDG and [^{68}Ga]Ga-CTR-FAPI PET-CT were processed using 3D slicer (version 4.11) and Python (version 3.8.5). Pathologic analysis was conducted using ImageJ (version 1.54 g). Statistical analyses were conducted in R (version 4.2.0).

Data Availability

The data generated in this study are available upon reasonable request from the corresponding author.

Authors' Disclosures

X.-Y. Cui reports a patent for "Trifunctional compound and use thereof" licensed to Boomray Radiopharmaceutical. Z. Liu reports other support from Boomray Radiopharmaceutical outside the submitted work; in addition, Z. Liu has a patent for "Trifunctional compound and use thereof" licensed to Boomray Radiopharmaceutical. No disclosures were reported by the other authors.

Authors' Contributions

Z. Kong: Data curation, formal analysis, funding acquisition, validation, investigation, visualization, methodology, writing–original draft, writing–review and editing. **Z. Li:** Data curation, funding acquisition, investigation, writing–original draft, writing–review and editing. **X.-Y. Cui:** Data curation, formal analysis, validation, methodology, writing–original draft, writing–review and editing. **J. Wang:** Data curation, formal analysis, investigation, writing–original draft, writing–review and editing. **M. Xu:** Data curation, methodology, writing–original draft, writing–review and editing. **Y. Liu:** Data curation, formal analysis, writing–original draft, writing–review and editing. **J. Chen:** Data curation, methodology, writing–review and editing. **S. Ni:** Data curation, investigation, writing–review and editing. **Z. Zhang:** Data curation, investigation, writing–review and editing. **X. Fan:** Data curation, methodology, writing–review and editing. **J. Huang:** Data curation, methodology, writing–review and editing. **Y. Lin:** Data curation, methodology, writing–review and editing. **Y. Sun:** Data curation, investigation, writing–review and editing. **Y. He:** Data curation, validation, writing–review and editing. **X. Lin:** Data curation, methodology, writing–review and editing. **T. Meng:** Data curation, methodology, writing–review and editing. **H. Li:** Data curation, investigation, writing–review and editing. **Y. Song:** Data curation, investigation, writing–review and editing. **B. Peng:** Data curation, investigation, writing–review and editing. **C. An:** Data curation, investigation, writing–review and editing. **C. Gao:** Resources, data curation, methodology, writing–review and editing. **N. Li:** Data curation, investigation, methodology, writing–review and editing. **C. Liu:** Data curation, investigation, methodology, writing–review and editing. **Y. Zhu:** Data curation, supervision, project administration, writing–review and editing. **Z. Yang:** Conceptualization, resources, data curation, validation, project administration, writing–review and editing. **Z. Liu:** Conceptualization, resources, data curation, supervision, funding acquisition, validation, writing–original draft, project administration, writing–review and editing. **S. Liu:** Conceptualization, resources, data curation, formal analysis, supervision, validation, investigation, methodology, project administration, writing–review and editing.

Acknowledgments

We thank all the patients and the referring physicians who made this study possible. We thank Dr. Feifei Jin for statistical assistance. This work was supported by the National Natural Science Foundation of China Grant No. 22225603 (Z. Liu) and No. 32301152 (Z. Kong), Beijing Municipal Natural Science Foundation Grant No. 7232351 (Z. Kong) and No. Z200018 (Z. Liu), Ministry of Science and Technology of the People's Republic of China Grant No. 2021YFA1601400 (Z. Liu), Science Foundation of Peking University Cancer Hospital Grant No. PY202309 (Z. Li), Peking University Clinical Scientist Training Program supported by the Fundamental Research Funds for the Central Universities No.BMU2024PYJH006 (Z. Li), CAMS Innovation Fund for Medical Sciences No. 2023-I2M-QJ-003 (S. Liu).

Note

Supplementary data for this article are available at Cancer Discovery Online (http://cancerdiscovery.aacrjournals.org/).

Received June 26, 2024; revised September 11, 2024; accepted October 25, 2024; published first October 29, 2024.

REFERENCES

1. Chen DW, Lang BHH, McLeod DSA, Newbold K, Haymart MR. Thyroid cancer. Lancet 2023;401:1531–44.
2. Fagin JA, Wells SA Jr. Biologic and clinical perspectives on thyroid cancer. N Engl J Med 2016;375:1054–67.
3. Boucai L, Zafereo M, Cabanillas ME. Thyroid cancer: a review. JAMA 2024;331:425–35.
4. Roman S, Lin R, Sosa JA. Prognosis of medullary thyroid carcinoma: demographic, clinical, and pathologic predictors of survival in 1252 cases. Cancer 2006;107:2134–42.
5. Maia AL, Wajner SM, Vargas CVF. Advances and controversies in the management of medullary thyroid carcinoma. Curr Opin Oncol 2017;29:25–32.
6. Machens A, Dralle H. Biomarker-based risk stratification for previously untreated medullary thyroid cancer. J Clin Endocrinol Metab 2010;95:2655–63.
7. Wells SA Jr, Asa SL, Dralle H, Elisei R, Evans DB, Gagel RF, et al. Revised American Thyroid Association guidelines for the management of medullary thyroid carcinoma. Thyroid 2015;25:567–610.
8. Leimbach RD, Hoang TD, Shakir MKM. Diagnostic challenges of medullary thyroid carcinoma. Oncology 2021;99:422–32.

9. Spanheimer PM, Ganly I, Chou JF, Capanu M, Nigam A, Ghossein RA, et al. Prophylactic lateral neck dissection for medullary thyroid carcinoma is not associated with improved survival. Ann Surg Oncol 2021;28:6572–9.
10. Hao W, Zhao J, Guo F, Zhang J, Gu P, Ruan X, et al. The survival outcomes of prophylactic lateral neck dissection for medullary thyroid carcinoma, a retrospective cohort study. Clin Otolaryngol 2023;48:734–9.
11. Kouvaraki MA, Shapiro SE, Fornage BD, Edeiken-Monro BS, Sherman SI, Vassilopoulou-Sellin R, et al. Role of preoperative ultrasonography in the surgical management of patients with thyroid cancer. Surgery 2003;134:946–54.
12. Treglia G, Cocciolillo F, Di Nardo F, Poscia A, de Waure C, Giordano A, et al. Detection rate of recurrent medullary thyroid carcinoma using fluorine-18 dihydroxyphenylalanine positron emission tomography: a meta-analysis. Acad Radiol 2012;19:1290–9.
13. Treglia G, Tamburello A, Giovanella L. Detection rate of somatostatin receptor PET in patients with recurrent medullary thyroid carcinoma: a systematic review and a meta-analysis. Hormones (Athens) 2017;16:362–72.
14. Terroir M, Caramella C, Borget I, Bidault S, Dromain C, El Farsaoui K, et al. F-18-Dopa positron emission tomography/computed tomography is more sensitive than whole-body magnetic resonance imaging for the localization of persistent/recurrent disease of medullary thyroid cancer patients. Thyroid 2019;29:1457–64.
15. Brammen L, Niederle MB, Riss P, Scheuba C, Selberherr A, Karanikas G, et al. Medullary thyroid carcinoma: do ultrasonography and F-DOPA-PET-CT influence the initial surgical strategy? Ann Surg Oncol 2018;25:3919–27.
16. Giraudet AL, Vanel D, Leboulleux S, Aupérin A, Dromain C, Chami L, et al. Imaging medullary thyroid carcinoma with persistent elevated calcitonin levels. J Clin Endocrinol Metab 2007;92:4185–90.
17. Romero-Lluch AR, Cuenca-Cuenca JI, Guerrero-Vázquez R, Martínez-Ortega AJ, Tirado-Hospital JL, Borrego-Dorado I, et al. Diagnostic utility of PET/CT with ^{18}F-DOPA and ^{18}F-FDG in persistent or recurrent medullary thyroid carcinoma: the importance of calcitonin and carcinoembryonic antigen cutoff. Eur J Nucl Med Mol Imaging 2017;44:2004–13.
18. Rubello D, Rampin L, Nanni C, Banti E, Ferdeghini M, Fanti S, et al. The role of ^{18}F-FDG PET/CT in detecting metastatic deposits of recurrent medullary thyroid carcinoma: a prospective study. Eur J Surg Oncol 2008;34:581–6.
19. Treglia G, Castaldi P, Villani MF, Perotti G, de Waure C, Filice A, et al. Comparison of ^{18}F-DOPA, ^{18}F-FDG and ^{68}Ga-somatostatin analogue PET/CT in patients with recurrent medullary thyroid carcinoma. Eur J Nucl Med Mol Imaging 2012;39:569–80.
20. Elisei R, Schlumberger MJ, Müller SP, Schöffski P, Brose MS, Shah MH, et al. Cabozantinib in progressive medullary thyroid cancer. J Clin Oncol 2013;31:3639–46.
21. Kreissl MC, Bastholt L, Elisei R, Haddad R, Hauch O, Jarząb B, et al. Efficacy and safety of vandetanib in progressive and symptomatic medullary thyroid cancer: post hoc analysis from the ZETA trial. J Clin Oncol 2020;38:2773–81.
22. Subbiah V, Hu MI, Wirth LJ, Schuler M, Mansfield AS, Curigliano G, et al. Pralsetinib for patients with advanced or metastatic RET-altered thyroid cancer (ARROW): a multi-cohort, open-label, registrational, phase 1/2 study. Lancet Diabetes Endocrinol 2021;9:491–501.
23. Subbiah V, Hu MI, Mansfield AS, Taylor MH, Schuler M, Zhu VW, et al. Pralsetinib in patients with advanced/metastatic rearranged during transfection (RET)-altered thyroid cancer: updated efficacy and safety data from the ARROW study. Thyroid 2024;34:26–40.
24. Hadoux J, Elisei R, Brose MS, Hoff AO, Robinson BG, Gao M, et al. Phase 3 trial of selpercatinib in advanced RET-mutant medullary thyroid cancer. N Engl J Med 2023;389:1851–61.
25. Giovanella L, Treglia G, Iakovou I, Mihailovic J, Verburg FA, Luster M. EANM practice guideline for PET/CT imaging in medullary thyroid carcinoma. Eur J Nucl Med Mol Imaging 2020;47:61–77.
26. Cheng X, Bao L, Xu Z, Li D, Wang J, Li Y. ^{18}F-FDG-PET and ^{18}F-FDG-PET/CT in the detection of recurrent or metastatic medullary thyroid carcinoma: a systematic review and meta-analysis. J Med Imaging Radiat Oncol 2012;56:136–42.
27. Ong SC, Schöder H, Patel SG, Tabangay-Lim IM, Doddamane I, Gönen M, et al. Diagnostic accuracy of 18F-FDG PET in restaging patients with medullary thyroid carcinoma and elevated calcitonin levels. J Nucl Med 2007;48:501–7.
28. Asa S, Sonmezoglu K, Uslu-Besli L, Sahin OE, Karayel E, Pehlivanoglu H, et al. Evaluation of F-18 DOPA PET/CT in the detection of recurrent or metastatic medullary thyroid carcinoma: comparison with GA-68 DOTA-TATE PET/CT. Ann Nucl Med 2021;35:900–15.
29. Hayes AR, Crawford A, Al Riyami K, Tang C, Bomanji J, Baldeweg SE, et al. Metastatic medullary thyroid cancer: the role of ^{68}Gallium-DOTA-somatostatin analogue PET/CT and peptide receptor radionuclide therapy. J Clin Endocrinol Metab 2021;106:e4903–16.
30. Haddad RI, Bischoff L, Ball D, Bernet V, Blomain E, Busaidy NL, et al. Thyroid carcinoma, version 2.2022, NCCN clinical practice guidelines in oncology. J Natl Compr Canc Netw 2022;20:925–51.
31. Kratochwil C, Flechsig P, Lindner T, Abderrahim L, Altmann A, Mier W, et al. ^{68}Ga-FAPI PET/CT: tracer uptake in 28 different kinds of cancer. J Nucl Med 2019;60:801–5.
32. Pang Y, Zhao L, Luo Z, Hao B, Wu H, Lin Q, et al. Comparison of ^{68}Ga-FAPI and ^{18}F-FDG uptake in gastric, duodenal, and colorectal cancers. Radiology 2021;298:393–402.
33. Koperek O, Scheuba C, Puri C, Birner P, Haslinger C, Rettig W, et al. Molecular characterization of the desmoplastic tumor stroma in medullary thyroid carcinoma. Int J Oncol 2007;31:59–67.
34. Kuyumcu S, Işık EG, Sanli Y. Liver metastases from medullary thyroid carcinoma detected on ^{68}Ga-FAPI-04 PET/CT. Endocrine 2021;74:727–8.
35. Al-Ibraheem A, Alyasjeen SF, Abdlkadir AS, Sheikha AA. [^{68}Ga]Ga-DOTA-FAPI-04 PET/CT depicts metastases from medullary thyroid cancer that [^{68}Ga]Ga-DOTATOC PET/CT missed. Eur J Nucl Med Mol Imaging 2023;50:4112–3.
36. Ballal S, Yadav MP, Roesch F, Raju S, Satapathy S, Sheokand P, et al. Head-to-Head comparison of [^{68}Ga]Ga-DOTA.SA.FAPi and [^{68}Ga]Ga-DOTANOC positron emission tomography/computed tomography imaging for the follow-up surveillance of patients with medullary thyroid cancer. Thyroid 2023;33:974–82.
37. Loktev A, Lindner T, Burger E-M, Altmann A, Giesel F, Kratochwil C, et al. Development of fibroblast activation protein-targeted radiotracers with improved tumor retention. J Nucl Med 2019;60:1421–9.
38. Cui X-Y, Li Z, Kong Z, Liu Y, Meng H, Wen Z, et al. Covalent targeted radioligands potentiate radionuclide therapy. Nature 2024;630:206–13.
39. Mona CE, Benz MR, Hikmat F, Grogan TR, Lückerath K, Razmaria A, et al. Correlation of ^{68}Ga-FAPi-46 PET biodistribution with FAP expression by immunohistochemistry in patients with solid cancers: a prospective translational exploratory study. J Nucl Med 2022;63:1021–6.
40. Subbiah V, Gainor JF, Rahal R, Brubaker JD, Kim JL, Maynard M, et al. Precision targeted therapy with BLU-667 for RET-driven cancers. Cancer Discov 2018;8:836–49.
41. Saqcena M, Leandro-Garcia LJ, Maag JLV, Tchekmedyian V, Krishnamoorthy GP, Tamarapu PP, et al. SWI/SNF complex mutations promote thyroid tumor progression and insensitivity to redifferentiation therapies. Cancer Discov 2021;11:1158–75.
42. Frank AR, Li V, Shelton SD, Kim J, Stott GM, Neckers LM, et al. Mitochondrial-encoded complex I impairment induces a targetable dependency on aerobic fermentation in hürthle cell carcinoma of the thyroid. Cancer Discov 2023;13:1884–903.
43. Gopal RK, Vantaku VR, Panda A, Reimer B, Rath S, To T-L, et al. Effectors enabling adaptation to mitochondrial complex I loss in hürthle cell carcinoma. Cancer Discov 2023;13:1904–21.
44. Haddad R, Elisei R, Hoff AO, Liu Z, Pitoia F, Pruneri G, et al. Diagnosis and management of tropomyosin receptor kinase fusion-positive thyroid carcinomas: a review. JAMA Oncol 2023;9:1132–41.
45. Shen C, Shi X, Wen D, Zhang Y, Du Y, Zhang Y, et al. Comprehensive DNA methylation profiling of medullary thyroid carcinoma: molecular classification, potential therapeutic target, and classifier system. Clin Cancer Res 2024;30:127–38.

46. Jiang J, Jiang L, Maldonato BJ, Wang Y, Holderfield M, Aronchik I, et al. Translational and therapeutic evaluation of RAS-GTP inhibition by RMC-6236 in RAS-driven cancers. Cancer Discov 2024;14:994–1017.
47. Schwartz LH, Litière S, de Vries E, Ford R, Gwyther S, Mandrekar S, et al. RECIST 1.1-update and clarification: from the RECIST committee. Eur J Cancer 2016;62:132–7.
48. Subbiah V, Cote GJ. Advances in targeting RET-dependent cancers. Cancer Discov 2020;10:498–505.
49. Selpercatinib shifts treatment paradigm for MTC and NSCLC. Cancer Discov 2023;13:OF8.
50. Calais J, Ceci F, Eiber M, Hope TA, Hofman MS, Rischpler C, et al. ^{18}F-fluciclovine PET-CT and ^{68}Ga-PSMA-11 PET-CT in patients with early biochemical recurrence after prostatectomy: a prospective, single-centre, single-arm, comparative imaging trial. Lancet Oncol 2019;20:1286–94.
51. Fendler WP, Calais J, Eiber M, Flavell RR, Mishoe A, Feng FY, et al. Assessment of ^{68}Ga-PSMA-11 PET accuracy in localizing recurrent prostate cancer: a prospective single-arm clinical trial. JAMA Oncol 2019;5:856–63.
52. Haugen BR, Alexander EK, Bible KC, Doherty GM, Mandel SJ, Nikiforov YE, et al. 2015 American thyroid association management guidelines for adult patients with thyroid nodules and differentiated thyroid cancer: the American thyroid association guidelines task force on thyroid nodules and differentiated thyroid cancer. Thyroid 2016;26:1–133.
53. Surasi DS, Eiber M, Maurer T, Preston MA, Helfand BT, Josephson D, et al. Diagnostic performance and safety of positron emission tomography with ^{18}F-rhPSMA-7.3 in patients with newly diagnosed unfavourable intermediate- to very-high-risk prostate cancer: results from a phase 3, prospective, multicentre study (LIGHTHOUSE). Eur Urol 2023;84:361–70.
54. Kong Z, Jiang C, Liu D, Chen W, Ma W, Cheng X, et al. Quantitative features from CHO PET distinguish the WHO grades of primary diffuse glioma. Clin Nucl Med 2021;46:103–10.